J|A|C|S ARTICLES

Published on Web 03/04/2010

Magnetic Glyco-Nanoparticles: A Tool To Detect, Differentiate, and Unlock the Glyco-Codes of Cancer via Magnetic Resonance Imaging

Kheireddine El-Boubbou,[†] David C. Zhu,[‡] Chrysoula Vasileiou,[†] Babak Borhan,[†] Davide Prosperi,[§] Wei Li,[⊥] and Xuefei Huang*[,†]

Departments of Chemistry, Radiology, and Psychology, Michigan State University, East Lansing, Michigan 48824, Department of Biotechnology and Bioscience, University of Milano-Bicocca, Piazza della Scienza 2, 20126 Milan, Italy, and College of Pharmacy, University of Tennessee Health Science Center, 847 Monroe Avenue, Memphis, Tennessee 38163

Received January 18, 2010; E-mail: xuefei@chemistry.msu.edu

Abstract: Within cancer, there is a large wealth of diversity, complexity, and information that nature has engineered rendering it challenging to identify reliable detection methods. Therefore, the development of simple and effective techniques to delineate the fine characteristics of cancer cells can have great potential impacts on cancer diagnosis and treatment. Herein, we report a magnetic glyco-nanoparticle (MGNP) based nanosensor system bearing carbohydrates as the ligands, not only to detect and differentiate cancer cells but also to quantitatively profile their carbohydrate binding abilities by magnetic resonance imaging (MRI). Using an array of MGNPs, a range of cells including closely related isogenic tumor cells, cells with different metastatic potential and malignant vs normal cells can be readily distinguished based on their respective "MRI signatures". Furthermore, the information obtained from such studies helped guide the establishment of strongly binding MGNPs as antiadhesive agents against tumors. As the interactions between glyco-conjugates and endogenous lectins present on cancer cell surface are crucial for cancer development and metastasis, the ability to characterize and unlock the glyco-code of individual cell lines can facilitate both the understanding of the roles of carbohydrates as well as the expansion of diagnostic and therapeutic tools for cancer.

Introduction

Cancer is a complex group of diseases that affect the lives of millions of people worldwide. Each malignant cell type has molecular signatures that distinguish it from its healthy counterpart. The availability of simple and fast methods to identify the unique cellular characteristics can greatly benefit cancer treatment and improve the clinical outcomes for patients.[1−3] Currently, the majority of methods for cancer detection target biomarkers such as mutated DNA/RNA and overexpressed antigens.[1,3−5] This requires extensive prior knowledge on the presence of the specific markers,[4,6] which can be very time-consuming to acquire. Furthermore, as tumor cells have high tendencies to mutate,[7,8] their antigenic variants may escape the detection leading to false negative results. An appealing alternative is to take advantage of cell surface receptor mediated recognition events. Receptor binding is often critical to cell functions and usually cannot be abolished without affecting cell viability. In addition, cell surface receptors would be easier to target without requiring the probes to cross the cellular membrane as compared to intracellular markers.

An attractive target for receptor-mediated interaction is carbohydrates and, in particular glycoconjugates, which play important roles in cancer development and metastasis.[9−12] Carbohydrates are uniquely suited for encoding biological information because of their rich structural variations.[13−15] Aberrant glycosylations on tumor cell surfaces have been

[†] Department of Chemistry, Michigan State University.
[‡] Departments of Radiology and Psychology, Michigan State University.
[§] University of Milano-Bicocca.
[⊥] University of Tennessee Health Science Center.

(1) Lee, H.; Yoon, T.-J.; Figueiredo, J.-L.; Swirski, F. K.; Weissleder, R. *Proc. Natl. Acad. Sci. U.S.A.* **2009**, *106*, 12459–12464.
(2) Bajaj, A.; Miranda, O. R.; Kim, I.-B.; Phillips, R. L.; Jerry, D. J.; Bunz, U. H. F.; Rotello, V. M. *Proc. Natl. Acad. Sci. U.S.A.* **2009**, *106*, 10912–10916, and references therein.
(3) Nagrath, S.; Sequist, L. V.; Maheswaran, S.; Bell, D. W.; Irimia, D.; Ulkus, L.; Smith, M. R.; Kwak, E. L.; Digumarthy, S.; Muzikansky, A.; Ryan, P.; Balis, U. J.; Tompkins, R. G.; Haber, D. A.; Toner, M. *Nature* **2007**, *450*, 1235–1239.
(4) Pantel, K.; Brakenhoff, R. H.; Brandt, B. *Nat. Rev. Cancer* **2008**, *8*, 329–340.
(5) Ludwig, J. A.; Weinstein, J. N. *Nat. Rev. Cancer* **2005**, *5*, 845–856.
(6) Ferrari, M. *Nat. Rev. Cancer* **2005**, *5*, 161–171.
(7) Hynes, N. E.; MacDonald, G. *Curr. Opin. Cell Biol.* **2009**, *21*, 177–184.
(8) Klein, C. A.; Blankenstein, T. J. F.; Schmidt-Kittler, O.; Petronio, M.; Polzer, B.; Stoecklein, N. H.; Riethmüller, G. *Lancet* **2002**, *360*, 683–689.
(9) Freire, T.; Bay, S.; Vichier-Guerre, S.; Lo-Man, R.; Leclerc, C. *Mini-Rev. Med. Chem.* **2006**, *6*, 1357–1373.
(10) Hakomori, S. *Proc. Natl. Acad. Sci. U.S.A.* **2002**, *99*, 10231–10233.
(11) Danishefsky, S. J.; Allen, J. R. *Angew. Chem., Int. Ed.* **2000**, *39*, 836–863, and references therein.
(12) Hakomori, S.; Zhang, Y. *Chem. Biol.* **1997**, *4*, 97–104.
(13) Gabius, H.-J. *Biochem. Soc. Trans.* **2008**, *36*, 1491–1496.
(14) Gabius, H.-J.; Siebert, H.-C.; André, S.; Jiménez-Barbero, J.; Rüdiger, H. *ChemBioChem* **2004**, *5*, 740–764.
(15) Varki, A. *Glycobiology* **1993**, *3*, 97–130.

 10.1021/ja100455c

extensively probed by antibodies and plant-derived lectins.[12,16] This led to the identification of characteristic tumor-associated carbohydrate molecules,[11,12] which has greatly facilitated the development of carbohydrate-based anticancer vaccine studies.[9,17] In comparison, the understanding of carbohydrate-binding properties of tumors is not as advanced. Cancer cells can interact with the extracellular matrix in their microenvironment through endogenous receptors binding with carbohydrates.[18−20] These interactions vary, depending on the physiological state of the cells, as supported by the ground-breaking histological studies of tumor tissues.[21−23] Therefore, the ability to characterize and distinguish carbohydrate binding profiles of a variety of cells can expedite both the mechanistic understanding of their roles in disease development and the expansion of diagnostic and therapeutic tools.[24−26] As the distinctions among cancer cell subtypes and malignant vs normal cells can often be subtle, a suitable tool is needed to *quantitatively* analyze the fine characteristics in carbohydrate binding of various cell types.

In the past decade, nanotechnology has begun to play increasingly important roles in cancer research.[6] Using antibody-immobilized nanoparticles, various types of cancer cells were detected both *in vitro*[1] and *in vivo*.[27] Recently, instead of relying on the specific antibodies, structurally related cationic gold nanoparticles bearing fluorescent polymers on the surface were prepared.[2] The differential electrostatic and hydrophobic interactions between the gold nanoparticles and cells were reflected in changes of fluorescence intensity upon cell binding, which allowed the differentiation of tumor from normal cells as well as closely related tumor cells. Herein, we explore the possibility of using a magnetic glyco-nanoparticle (MGNP)-based system to detect and profile various cell types on the basis of the more physiologically related carbohydrate−receptor interactions. MGNPs provide an appealing platform for biological detection. The spherical nanoparticles have large surface areas, which allow the attachment of multiple carbohydrates leading to enhanced avidity with carbohydrate receptors through multivalent binding.[13,28] Unlike the toxic heavy metal-containing nanoparticles such as quantum dots,[29,30] the magnetite nanoparticles have been approved for clinical uses with minimum cytotoxicity.[31] Furthermore, the superparamagnetic nature of this MGNPs can allow cell detection via magnetic resonance imaging (MRI) without the need to prelabel the cells.[31−33]

One challenge, however, in using MGNPs and carbohydrates for molecular recognition is that multiple cell types may bind with the same carbohydrate structure albeit in different affinities. To address this issue, we envision that by pooling the responses from an array of MGNPs, the various cell types may be differentiated through pattern recognition.[2,34−36] Furthermore, the information obtained on the physiologically relevant carbohydrate−receptor interaction can not only enhance our understanding of the roles carbohydrate play in cancer but also guide the development of potential therapeutics such as agents against cancer adhesion. Although glyco-nanoparticles have been previously employed for elegant studies of carbohydrate-mediated biological recognitions,[37−48] MGNPs have not been utilized to detect and systematically profile mammalian cells.

Experimental Section

Cells and Culture Conditions. Unless otherwise indicated, all starting materials, reagents and solvents were obtained from commercial suppliers (Sigma-Aldrich or Fisher Scientific) and used as supplied without further purification. All fluorescein-labeled lectins were purchased from Aldrich. All cell lines were purchased from the American Type Culture Collection (ATCC) [cell line designation (catalogue no.), type] unless otherwise noted: 184B5 (CRL-8799), normal breast cell; A498 (HTB-44), kidney cancer; A549 (CCL-185), lung cancer; HT29 (HTB-38), colon cancer; SKOV-3 (HTB-77), ovarian cancer; B16-F10 (CRL-6475), metastatic mouse melanoma; B16-F1 (CRL-6323), less metastatic mouse melanoma. The MCF-7/Adr-res (adriamycin-resistant breast cancer) cell line was obtained from the National Cancer Institute. Two murine mammary carcinoma cell lines (TA3-HA, TA3-ST) were kind gifts from Dr. John Hilkens, Netherlands Cancer Institute. All

(16) Dai, Z.; Zhou, J.; Qiu, S.-J.; Liu, Y.-K.; Fan, J. *Electrophoresis* **2009**, *30*, 2957–2966, and references therein.
(17) Buskas, T.; Thompson, P.; Boons, G.-J. *Chem. Commun.* **2009**, 5335–5349.
(18) Barthel, S. R.; Gavino, J. D.; Descheny, L.; Dimitroff, C. J. *Exp. Opin. Ther. Targets* **2007**, *11*, 1473–1491.
(19) Kannagi, R.; Izawa, M.; Koike, T.; Miyazaki, K.; Kimura, N. *Cancer Sci.* **2004**, *65*, 377–384.
(20) Lahm, H.; Andre, S.; Hoeflich, A.; Kaltner, H.; Siebert, H.-C.; Sordat, B.; von der Lieth, C.-W.; Wolf, E.; Gabius, H.-J. *Glycoconjugate J.* **2004**, *20*, 227–238.
(21) Gabius, H.-J. *Anat. Histol. Embryol.* **2001**, *30*, 3–31, and references therein.
(22) Kayser, K.; Bovin, N. V.; Zemlyanukhina, T. V.; Donaldo-Jacinto, S.; Koopmann, J.; Gabius, H.-J. *Glycoconjugate J.* **1994**, *11*, 339–344.
(23) Kayser, K.; Heil, M.; Gabius, H.-J. *Pathol., Res. Pract.* **1989**, *184*, 621–629.
(24) Kim, E. Y. L.; Gronewold, C.; Chatterjee, A.; Von der Lieth, C.-W.; Kliem, C.; Schmauser, B.; Wiessler, M.; Frei, E. *ChemBioChem* **2005**, *6*, 422–431 and references cited therein.
(25) Lerchen, H.-G.; Baumgarten, J.; Piel, N.; Kolb-Bachofen, V. *Angew. Chem., Int. Ed.* **1999**, *38*, 3680–3683.
(26) Rye, P. D.; Bovin, N. V. *Glycobiology* **1997**, *7*, 179–182.
(27) Gao, X.; Cui, Y.; Levenson, R. M.; Chung, L. W. K.; Nie, S. *Nat. Biotechnol.* **2004**, *22*, 969–979.
(28) Lee, Y. C.; Lee, R. T. *Acc. Chem. Res.* **1995**, *28*, 321–327.
(29) Chang, E.; Thekkek, N.; Yu, W. W.; Colvin, V. L.; Drezek, R. *Small* **2006**, *2*, 1412–1417.
(30) Derfus, A. M.; Chan, W. C. W.; Bhatia, S. N. *Nano Lett.* **2004**, *4*, 11–18.
(31) Gupta, A. K.; Gupta, M. *Biomaterials* **2005**, *26*, 3995–4021.
(32) Wang, Y.-X. J.; Hussain, S. M.; Krestin, G. P. *Eur. Radiol.* **2001**, *11*, 2319–2331.
(33) Weissleder, R.; Elizondo, G.; Wittenberg, J.; Rabito, C. A.; Bengele, H. H.; Josephson, L. *Radiology* **1990**, *175*, 489–493.
(34) Collins, B. E.; Wright, A. T.; Anslyn, E. V. *Top. Curr. Chem.* **2007**, *277*, 181–218.
(35) Wright, A. T.; Anslyn, E. V. *Chem. Soc. Rev.* **2006**, *35*, 14–28.
(36) Jurs, P. C.; Bakken, G. A.; McClelland, H. E. *Chem. Rev.* **2000**, *100*, 2649–2678.
(37) Barrientos, A. G.; de la Fuente, J. M.; Jiménez, M.; Solís, D.; Cañada, F. J.; Martín-Lomas, M.; Penadés, S. *Carbohydr. Res.* **2009**, *344*, 1474–1478.
(38) Liang, C.-H.; Wang, C.-C.; Lin, Y.-C.; Chen, C.-H.; Wong, C.-H.; Wu, C.-Y. *Anal. Chem.* **2009**, *81*, 7750–7756.
(39) Marradi, M.; Alcántara, D.; de la Fuente, J. M.; García-Martín, M. L.; Cerdán, S.; Penadés, S. *Chem. Commun.* **2009**, 3922–3924.
(40) van Kasteren, S. I.; Campbell, S. J.; Serres, S.; Anthony, D. C.; Sibson, N. R.; Davis, B. G. *Proc. Natl. Acad. Sci. U.S.A.* **2009**, *106*, 18–23.
(41) Kikkeri, R.; Lepenies, B.; Adibekian, A.; Laurino, P.; Seeberger, P. H. *J. Am. Chem. Soc.* **2009**, *131*, 2110–2112.
(42) Thygesen, M. B.; Sauer, J.; Jensen, K. J. *Chem.−Eur. J.* **2009**, *15*, 1649–1660.
(43) Mukhopadhyay, B.; Martins, M. B.; Karamanska, R.; Russell, D. A.; Field, R. A. *Tetrahedron Lett.* **2009**, *50*, 886–889.
(44) Sundgren, A.; Barchi, J. J. *Carbohydr. Res.* **2008**, *343*, 1594–1604.
(45) El-Boubbou, K.; Gruden, C.; Huang, X. *J. Am. Chem. Soc.* **2007**, *129*, 13392–13393.
(46) de Souza, A. C.; Halkes, K. M.; Meeldijk, J. D.; Verkleij, A. J.; Vliegenthart, J. F. G.; Kamerling, J. P. *ChemBioChem* **2005**, *6*, 828–831.
(47) Hone, D. C.; Haines, A. H.; Russell, D. A. *Langmuir* **2003**, *19*, 7141–7144.
(48) Lin, C.-C.; Yeh, Y.-C.; Yang, C.-Y.; Chen, G.-F.; Chen, Y.-C.; Wu, Y.-C.; Chen, C.-C. *Chem. Commun.* **2003**, 2920–2921.

Scheme 1. Synthesis of MGNPs

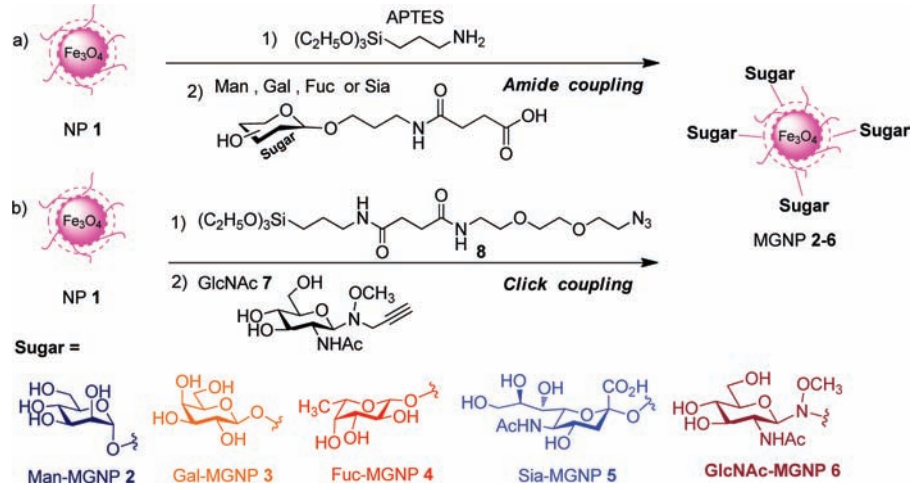

cell lines were grown as monolayer cultures on tissue culture dishes in phenol red free DMEM (Invitrogen, Carlsbad, CA) supplemented with 10% fetal bovine serum (FBS) (Sigma), penicillin G (Sigma, 61.4 μg/mL), streptomycin (Sigma, 100 μg/mL) and L-glutamine (Sigma, 292 μg/mL) at 37 °C in an atmosphere of 5% CO_2 and 95% air. All cells were grown to log phase, trypsinized with trypsin−EDTA solution (0.25% trypsin, 1 mM EDTA) to detach the cells, washed twice by centrifugation to remove any residual trypsin, and resuspended in the appropriate media.

HR-MAS ^{1}H NMR Analyses. HR-MAS experiments were carried out on a Bruker BioSpin FT-NMR Avance 500 equipped with an 11.7 T superconducting ultrashield magnet available at C.IGA (Centro Interdipartimentale Grandi Apparecchiature) of the University of Milan. The HR-MAS probe with internal lock is capable of performing either direct or indirect (inverse) detection experiments. MAS experiments were performed at spinning rates of up to 15 kHz (15 kHz maximum MAS rotation available) using a 50 μL zirconia rotor. All the samples were diluted at different concentrations with deuterated solvents to find out the concentration limit to the NMR signal broadening. HR-MAS ^{1}H NMR spectra were obtained using 200−400 scans for each experiment. The sample temperature was dependent on the rotation speed.

MRI and Relaxivity Measurement. Magnetic resonance imaging studies were carried on a 3T Signa HDx MR scanner (GE Healthcare, Waukesha, WI). Thirty test tube samples were scanned simultaneously in a standard quadrature birdcage head coil. For $T2$ measurements, a multiecho fast spin−echo sequence (time of repetition = 500 ms, receiver bandwidth = ± 31.25 kHz, field of view = 20 cm, slice thickness = 3 mm, gap = 3 mm, number of excitation = 1, and matrix size = 256 × 128) was used to simultaneously collect a series of data points at seven different echo times (TE) 15−60 ms with an increment of 7.5 ms at two slice locations. For each sample, the region of interest (ROI) (circles of 4.5 mm radius) was drawn at the center of each test tube at both slice locations. The $T2$ was calculated on the basis of the semilog linear regression of the mean signal intensity values at the ROI and the corresponding TEs. Specifically, $1/T2 = -[(\ln S_n - \ln S_m)/(TE_n - TE_m)]$, where S_n and S_m are voxel signal intensity values at TE values of TE_n and TE_m.

Detection of Cancer Cells using MGNPs. Cell suspensions (10^5 or 10^6 cells/mL) were prepared in phenol red free DMEM media supplemented with 0.2% bovine serum albumin. Aliquots of these cultures were placed in sterile tubes, and MGNPs **2**−**6** (final concentration 20 μg/mL) were added. NP **1** without any carbohydrates was used as the control. The tubes were incubated with gentle mixing at 37 °C. The $T2$ values of MGNP/cell suspensions and MGNP in the absence of cells were then recorded via MRI. MRI experiments were performed eight times for each cell line at both cell concentrations. The largest $T2$ value change upon binding with cells for each MGNP was set as 100%. The $\Delta T2$% for each cell line was calculated as the percentage of change relative to the largest $T2$ changes for the respective MGNP. LDA was performed using the statistical computing and graphics software R.

Prussian Blue Staining. Different cancer cell lines were seeded onto 24-well plate. After incubation for 12 h at 37 °C, nanoparticles were added to the plate in a final concentration of 20 μg/mL per well. After 12 h, the supernatant was removed, and cells were washed three times with PBS, treated with 10% formalin solution (0.5 mL) for 5 min to fix the cells, and then washed with PBS. Prussian blue staining was then performed. To each well was added a 1:1 mixture of 4% potassium ferrocyanide(II) trihydrate and 2% HCl solution (0.5 mL), and cells were incubated for 30 min at 37 °C in the dark, counterstained with nuclear fast red for 3 min, and then washed three times with PBS. The Prussian blue staining images were assessed by an inverted light microscope (Figures 6 and S9 (Supporting Information)).

Antiadhesive Assay. Cancer cells were detached using 2 mM EDTA in PBS, washed with PBS, counted to final concentration of ~5×10^4 cells/mL and incubated with Gal-MGNP (20 μg/mL) for 3 h at 37 °C in DMEM containing 10% FBS. The cells were then immediately seeded in a 24-well plate and incubated at 37 °C. After 10, 20, 30, and 45 min of incubation, the medium and the floating cells were carefully removed by aspiration, and the attached layers were washed twice with PBS. The firmly attached cells were then counted under an inverted light microscope. Cell adhesion curves were generated after counting triplicate wells (20 different homogeneous fields per each well). The same experiment was also performed at a different cell density of ~5×10^5 cells/mL (Figure S11, Supporting Information).

Results and Discussion

Synthesis and Characterization of MGNPs. The synthesis of MGNPs commenced from the tetraethoxysilane coated magnetite nanoparticle (NP **1**),[45,49] on which amino groups were introduced via silanization with 3-aminopropyl triethoxysilane (APTES) (Scheme 1a). Carboxylic acid derivatives of four types of naturally occurring monosaccharides, namely, mannose (Man), galactose (Gal), fucose (Fuc), and sialic acid (Sia), were then immobilized onto the amine-functionalized nanoparticles through amide coupling reactions leading to MGNP **2**−**5**, respectively (Scheme 1a).

In an alternative method, we synthesized GlcNAc-MGNP **6** via click chemistry. To this end, we explored the possibility of using a native unprotected sugar. The free reducing sugar

(49) Srinivasan, B.; Huang, X. *Chirality* **2008**, *20*, 265–277.

Scheme 2[a]

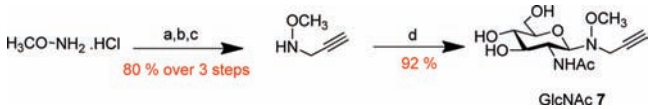

[a] Reagents and conditions: a) Benzoyl chloride, pyridine, CH_2Cl_2, 0 °C to rt, 2 h; b) 3-bromopropyne, K_2CO_3, acetone, reflux for 8 h; c) 6% MeOH in HCl, reflux for 2 h; d) *N*-acetyl glucosamine, 0.1 M acetate buffer (pH = 6.5)/DMF (3:1), 50 °C, 24 h.

N-acetyl glucosamine (GlcNAc) was chemoselectively ligated with a methoxy amine linker producing GlcNAc derivative **7** containing a terminal alkyne at the reducing end (Scheme 2).[50,51] NP **1** was then modified with the azido siloxane derivative **8** (see Scheme S4 for synthetic details (Supporting Information)), which was subsequently coupled with alkynyl-GlcNAc **7** through the copper-catalyzed Huisgen click reaction[52−54] to yield GlcNAc-MGNP **6** (Scheme 1b). It is advantageous to use a native unprotected sugar as this opens up an avenue for future incorporation of natural polysaccharides without extensive synthetic manipulations.

All NPs assembled were characterized by a variety of techniques, including transmission electron microscopy (TEM), nuclear magnetic resonance (NMR), thermogravimetric analysis (TGA), infrared spectroscopy, and X-ray diffraction (Figures S1−S3, Supporting Information). TEM images of MGNPs indicated that the diameters of NPs were around 6 nm (Figure 1a) and TGA showed that about 8% of the dry weight of MGNPs was due to carbohydrates (Figure S1, Supporting Information). NMR is a critical tool for providing detailed ligand structural features. Unfortunately, there is a serious limitation directly applying ^{1}H NMR to MGNPs due to the field inhomogeneity caused by the inherent superparamagnetism of the particles. Drastic line broadening was observed in spectra recorded with a conventional NMR probe, which led to undistinguishable ^{1}H NMR spectra (Figure 1b). Recently, high resolution-magic angle spinning (HR-MAS) NMR was found to be a superior tool to overcome this problem.[52,55] Indeed, HR-MAS ^{1}H NMR spectra of MGNPs gave solution- like spectra with a completely resolved splitting pattern, including the correct signal multiplicities and accurate integrations (Figure 1c). For instance, the anomeric proton of the galactoside ligand on Gal-MGNP **3** was well resolved as a doublet (J = 8.0 Hz) at 4.3 ppm, indicating the configuration of the carbohydrate was unaffected during immobilization. The fact that only one set of peaks from carbohydrates was observed suggested that the carbohydrate coating was homogeneous on the particle surface.

Validation of MGNP-Binding Specificities. Although glyconanoparticles have been previously utilized to probe carbohydrate−receptor interactions,[37−48] it is important to validate that the carbohydrates immobilized on MGNPs retain their biological recognition specificity. This was probed using four lectins, i.e., *Concanavalin A* (Con A, a Man selective lectin),[56] *Wheat Germ Agglutinin* (WGA, a GlcNAc and Sia selective lectin),[57,58] a *Bandeiraea simplicifolia* isolectin (BS-I, a Gal selective lectin)[59] and Lotus *Tetragonolobus purpureas Agglutinin* (TPA, a Fuc-selective lectin).[60] Upon incubation of a fluorescently labeled lectin with a MGNP, if the MGNP can bind with the lectin, subsequent application of an external magnetic field to the sample would remove the fluorescent lectin from the solution, leading to a reduction of fluorescent intensity of the supernatant. (For complete results on all five MGNPs binding with the four lectins, see Figures S4 and S5 (Supporting Information).) Con A is a well-characterized Man selective lectin with weak Gal-binding affinities.[56] Incubation of Man MGNP **2** (1 mg/mL) with fluorescein isocyanate (FITC)-labeled Con A (100 μg/mL) followed by magnetic separation led to a 89% reduction in fluorescent intensity of the solution, while the same amount of the weakly bound Gal-MGNP **3** was able to remove only 8% of the Con A (Figure 2a). This is consistent with the known carbohydrate binding preferences of Con A.[56] The addition of a solution of free mannose (18 mg/mL, 100 mM) to Man-MGNP **2**/Con A mixture did not increase the intensity of residual emission of the supernatant after magnetic separation and high concentration of mannose (180 mg/mL, 1 M) was required to partially disrupt the Con A/Man-MGNP **2** complex. These results reveal that multivalent display of carbohydrate ligands on MGNP resulted in strong lectin binding.

In contrast to Con A, the Gal-selective FITC-BS-I[59] strongly bound with Gal-MGNP **3**, producing 91% reduction of the solution emission intensity, which was competitively inhibited by a concentrated solution of free galactose (Figure 2b). At the same time, as BS-I has weak affinities with mannose,[59] incubation of Man-MGNP **2** with FITC-BS-I only decreased emission intensity a little. The same phenomena were observed with WGA and TPA (Figure S4, Supporting Information). WGA bound tightly with GlcNAc-MGNP **6** and Sia-MGNP **5** but not with Gal-MGNP **3** and TPA interacted strongly with Fuc-MGNP **4** as predicted on the basis of their known binding specificities.[57,58,60,61] In addition, NP **1** devoid of carbohydrates on the surface could not remove any proteins from the solution, suggesting that the nonspecific absorption on NP surface is minimal.

To further validate the specificity, we investigated the interactions of MGNP with a well-characterized *Escherichia coli* system. The *E. coli* strain ORN178 contains the mannose binding protein FimH in its fimbriae, while the ORN208 strain has its FimH mutated, resulting in much reduced mannose affinity.[62] Upon incubation of the ORN178 strain with Man-MGNP **2** and subsequent magnetic separation, close to 85% of the bacteria was removed from the media (Figure S6, Supporting Information).[45] In comparison, the mutant strain ORN208 bound with Man-MGNP **2** weakly, only losing 8% of the cells. Meanwhile, the Gal-MGNP **3** was ineffective in removing either strain. These observations coupled with the lectin experiments unequivocally demonstrated that the MGNPs are not promiscu-

(50) Bohorov, O.; Andersson-Sand, H.; Hoffmann, J.; Blixt, O. *Glycobiology* **2006**, *16*, 21C–27C.
(51) Peri, F.; Jiménez-Barbero, J.; García-Aparicio, V.; Tvaroška, I.; Nicotra, F. *Chem.—Eur. J.* **2004**, *10*, 1433–1444.
(52) Polito, L.; Monti, D.; Caneva, E.; Delnevo, E.; Russo, G.; Prosperi, D. *Chem. Commun.* **2008**, 621–623.
(53) Lin, P.-C.; Ueng, S.-H.; Yu, S.-C.; Jan, M.-D.; Adak, A. K.; Yu, C.-C.; Lin, C.-C. *Org. Lett.* **2007**, *9*, 2131–2134.
(54) Wang, Q.; Chan, T. R.; Hilgraf, R.; Fokin, V. V.; Sharpless, K. B.; Finn, M. G. *J. Am. Chem. Soc.* **2003**, *125*, 3192–3193.
(55) Polito, L.; Colombo, M.; Monti, D.; Melato, S.; Caneva, E.; Prosperi, D. *J. Am. Chem. Soc.* **2008**, *130*, 12712–24.
(56) Shimura, K.; Kasai, K. *Anal. Biochem.* **1995**, *227*, 186–194.
(57) Nagata, Y.; Burger, M. M. *J. Biol. Chem.* **1974**, *249*, 3116–3122.
(58) Vornholt, W.; Hartmann, M.; Keusgen, M. *Biosen. Bioelectron.* **2007**, *22*, 2983–2988.
(59) Hayes, C. E.; Goldstein, I. J. *J. Biol. Chem.* **1974**, *249*, 1904–1914.
(60) Liener, I. E., Sharon, N., Goldstein, I. J., Eds. *The Lectins: Properties, Functions, and Applications in Biology and Medicine*; Academic Press: Orlando, FL, 1986.
(61) Wright, C. S. *J. Mol. Biol.* **1984**, *178*, 91–104.
(62) Harris, S. L.; Spears, P. A.; Havell, E. A.; Hamrick, T. S.; Horton, J. R.; Orndorff, P. E. *J. Bacteriol.* **2001**, *183*, 4099–4102.

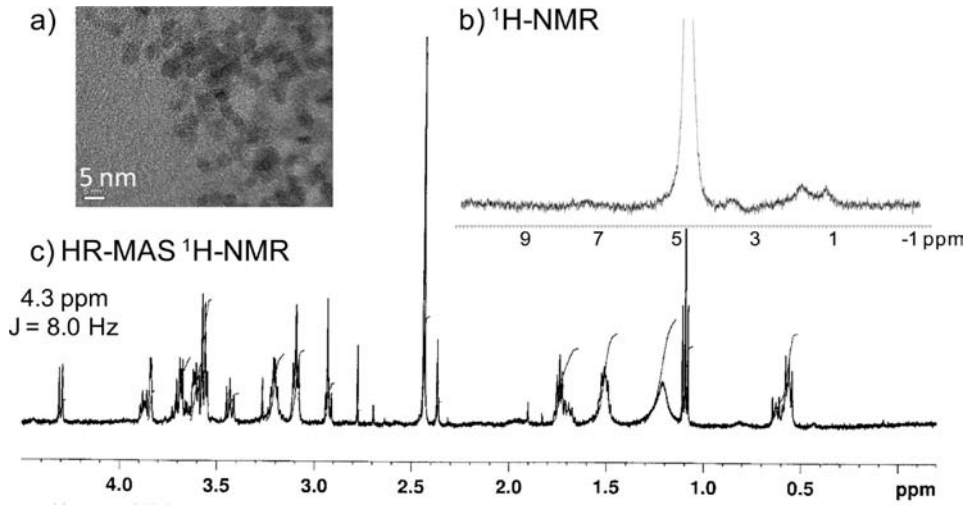

Figure 1. (a) TEM of Gal-MGNP **3** (the scale bar is 5 nm); (b) ^{1}H NMR spectrum of Gal-MGNP **3** acquired in solution with a conventional 5 mm probe (QNP); and (c) HR-MAS ^{1}H NMR of the same sample.

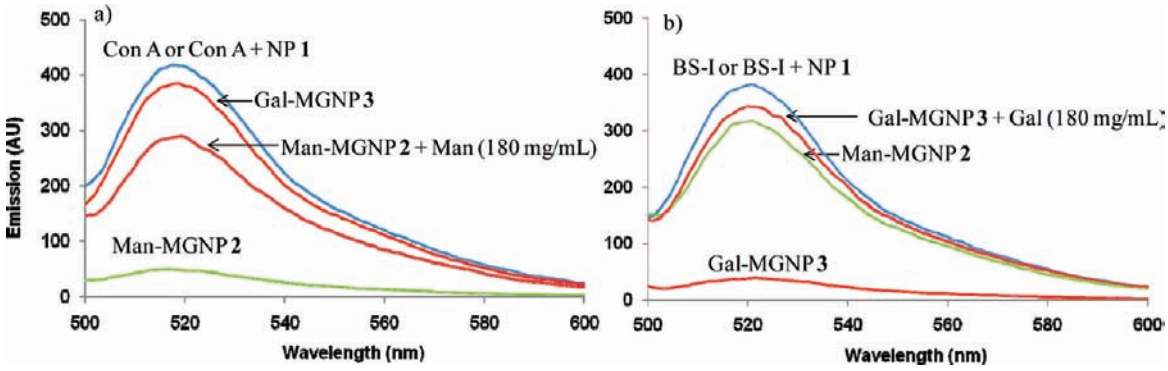

Figure 2. Fluorescent emission intensities of supernatants of (a) FITC-Con A (100 μg/mL) and (b) FITC-BS-I (100 μg/mL) upon incubation with various MGNPs (1 mg/mL) followed by magnet-mediated separation ($\lambda_{excitation}$ = 494 nm). Man-MGNP **2** bound strongly with the Man-selective Con A but not with Gal-selective BS-I, while Gal-MGNP **3** bound tightly with BS-I but not with Con A. The binding between lectins and the specfic MGNP could be competitively inhibited with a concentrated solution of the same carbohydrate.

ous in binding and the carbohydrates immobilized on MGNPs maintain the same biological recognition preference as the free forms in solution.

Monitoring MGNP Binding by MRI. After establishing the specificity of MGNPs using fluorescence experiments, we moved on to examine the utility of MRI to monitor the interaction of MGNPs with their biological targets. MRI measures the relaxation time of water protons in a magnetic field, which is commonly used to noninvasively visualize the internal structures and functions *in vivo*. Using MRI to monitor MGNP allows multiple samples to be measured simultaneously within a single scan,[63] thus enabling rapid response time and shortening multianalyte data acquisition. Furthermore, when the MRI methodology for MGNP monitoring is established, it can be translated to *in vivo* applications without the need to develop a new detection technology.

Magnetic NPs can serve as MRI contrast agents, where they decrease the transverse relaxation time (*T*2), producing a negative contrast from the environment by virtue of signal reduction.[32,64,65] In the presence of a cross-linking receptor, due to the small sizes of MGNPs, multiple MGNPs can bind with the receptor, assembling into clusters (Figure 3). With their increased sizes, the aggregates create larger local magnetic field gradients and thus become more efficient at dephasing the spins of surrounding water protons as the motional averaging condition is satisfied at the nanoparticle size regime.[66,67] This leads to lowering of *T*2 relaxation times as described by the magnetic relaxation switching theory.[1,63,68]

Our detection assay was first tested using Con A. As one Con A contains four mannose binding sites,[69] it can cross-link multiple mannose containing Man-MGNP **2**, leading to NP aggregation, which should result in the reduction of *T*2 relaxation time (Figure 3a). Due to the superparamagnetic nature of the magnetic nanoparticles, only 20 μg/mL of MGNP was needed for detection. When Man-MGNP **2** was mixed with increasing concentrations of Con A, the binding equilibrium was shifted more toward the aggregates. This led to a sequential decrease of the brightness of the corresponding *T*2-weighted

(63) Lee, H.; Sun, E.; Ham, D.; Weissleder, R. *Nat. Med.* **2008**, *14*, 869–874.
(64) Thorek, D. L. J.; Chen, A. K.; Czupryna, U.; Tsourkas, A. *Ann. Biomed. Eng.* **2005**, *34*, 23–38.
(65) Weissleder, R.; Papisov, M. *Rev. Magn. Reson. Med* **1992**, *4*, 1–20.
(66) Rocha, A.; Gossuinb, Y.; Mullera, R. N.; Gillis, P. *J. Magn. Magn. Mater.* **2005**, *293*, 532–539.
(67) Yung, K.-T. *Magn. Reson. Imaging* **2003**, *21*, 451–463.
(68) Koh, I.; Hong, R.; Weissleder, R.; Josephson, L. *Angew. Chem., Int. Ed.* **2008**, *47*, 4119–4121.
(69) Derewenda, Z.; Yariv, J.; HelliweII, J. R.; Kalb, A. J.; Dodson, E. J.; Papiz, M. Z.; Wan, T.; Campbell, J. *EMBO J.* **1989**, *8*, 2189–2193.

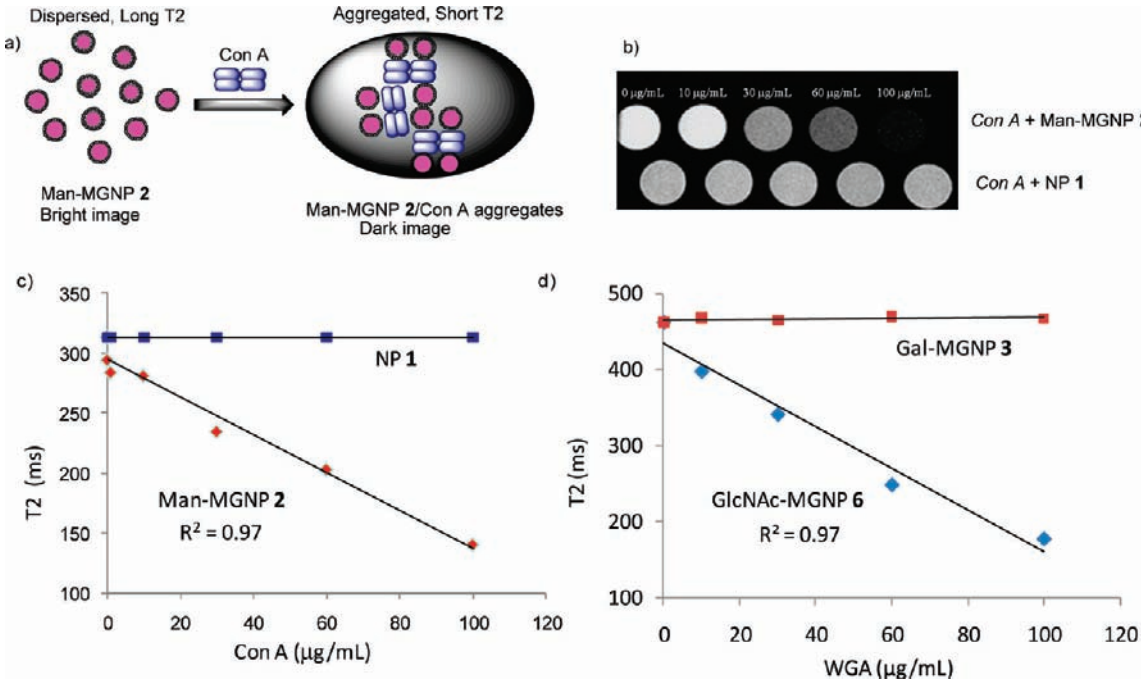

Figure 3. (a) Incubation of Man-MGNP **2** (shown as pink balls) with Con A, a tetrameric mannose selective lectin (shown as blue rectangles) resulted in the formation of aggregates, leading to shorter *T*2 relaxation time and consequently a darkened MRI image. (b) *T*2-weighted MRI images of Man-MGNP **2** (20 μg/mL) and NP **1** (20 μg/mL) upon incubation with increasing concentrations of Con A. (c) *T*2 changed linearly upon incubation of Man-MGNP **2** with increasing concentrations of Con A, while incubation with NP **1** devoid of carbohydrates did not lead to any change. (d) *T*2 changed linearly upon incubation of GlcNAc-MGNP **6** with increasing concentrations of the GlcNAc-selective lectin WGA, while incubation with the nonbinding Gal-MGNP **3** did not cause any *T*2 change.

MR images (Figure 3b). Quantification of the images showed an excellent linear correlation between Con A concentration and *T*2 relaxation time, with as little as 0.1 μg/mL (1 nM) of Con A detected (Figure 3c). In contrast, the control NP **1** devoid of mannose did not cause any change in *T*2, signifying that the contrast change was due to the specific binding between Man-MGNP **2** and Con A. In addition, incubation of the GlcNAc selective WGA with GlcNAc-MGNP **6** led to a linear decrease of *T*2 relaxation time with increasing concentrations of WGA, while the mixture of WGA with the nonbinding Gal-MGNP **3** did not produce any *T*2 changes (Figure 3d). These results corroborated the fluorescence studies and confirmed MGNP binding specificities (Figures 2, S4, S6, and S7 (Supporting Information)), which gave us great confidence to apply this technology to cancer cell study.

Mammalian Cells Selectively Bound with MGNPs As Detected by MRI. Building on the success of lectin and *E. coli* detection, we evaluated the utility of MGNPs in monitoring mammalian cell interactions and cancer cell detection. The use of carbohydrates as the recognition elements can provide functional information on cell surface active carbohydrate receptors. This is complementary to the usage of antibodies, as the latter monitor the presence of particular antigenic structures, which can be absent in some cancer cell mutants. In addition, an antibody is commonly limited to binding a specific target, while carbohydrate ligands can be used to monitor a range of cells, thus reducing the number of reagents required for study.

A normal breast cell line 184B5 and nine types of representative cancer cells were used for our study including human ovarian adenocarcinoma SKOV-3, colon HT29, kidney A498, lung A549, and breast cancer MCF-7/Adr-res and the closely related murine melanoma cell lines B16F10 and B16F1, mammary adenocarcinoma TA3-ST and TA3-HA. Each type of cells at two concentrations (10^5 and 10^6 cells/mL) was incubated with MGNP **2**−**6** or the control NP **1**, and the *T*2 relaxation times of all the samples were recorded. Thirty samples were measured at the same time with our MRI setup. While no significant *T*2 changes were observed with any cells upon mixing with the NP **1**, the 10 cell lines produced a large variation in *T*2 reductions upon MGNP incubation with the *T*2 changes normalized against the largest $\Delta T2$ within each MGNP category (Figure 4).

The decrease of the absolute values of *T*2 upon MGNP incubation can be explained due to particle agglomeration upon cell binding. At a higher cell concentration (10^6 cells/mL, Figure 4b), more MGNPs were bound leading to larger $\Delta T2$ compared with lower cell concentration (10^5 cells/mL) for each cell line (Figure 4a). Furthermore, when the cells were preincubated with a solution of a free monosaccharide (100 mM) and then treated with the MGNP bearing the same carbohydrate, *T*2 changes were less due to the competitive binding of the free monosaccharide with cells. These observations were consistent with the notion that *T*2 reduction was induced by the specific MGNP/cell interactions.

Biological Implications of Carbohydrate-Receptors on Cancer Cells. Based on the MR responses, in most of the cell lines examined, bindings with Fuc-MGNP **4** and Sia-MGNP **5** were observed (Figure 4), suggesting these cell lines have active fucose and sialic acid receptors. B16F1, B16F10, MCF-7/Adr-res, and SKOV-3 were found to interact with β-galactoside. This is of special interest since it confirmed the previously reported galactoside binding of the B16F10[24] presumably through galectins, a family of galactose specific lectins as well as the

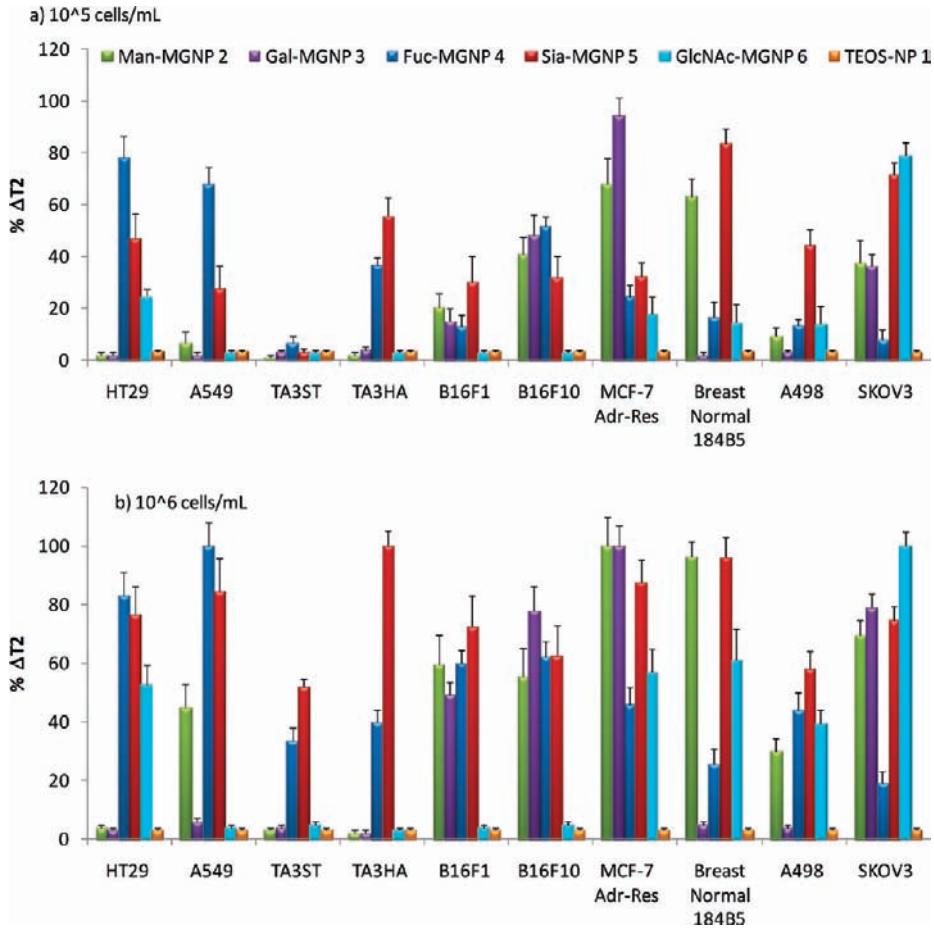

Figure 4. (a) Percentage changes of *T*2 relaxation time (% Δ*T*2) obtained upon incubating MGNPs **2**−**6** or the control NP **1** (20 μg/mL) with 10 cell lines (10^5 cells/mL). The Δ*T*2 was calculated by dividing the *T*2 differences between MGNP and MGNP/cancer cell by the corresponding highest Δ*T*2 from each MGNP category. (b) % Δ*T*2 obtained upon incubating MGNPs **2**−**6** or the control NP **1** (20 μg/mL) with 10 cell lines (10^6 cells/mL). The above data represent the averages of eight individual measurements with the error bars showing standard deviations.

high expression level of galectins on MCF-7/Adr-res[70] cells. Furthermore, HT29, MCF-7/Adr-res, 184B5, A498, and SK-OV-3 express functioning GlcNAc receptors as suggested by their interactions with GlcNAc-MGNP **6**. Moreover, MCF-7/Adr-res, 184B5, SKOV-3, B16F10, B16F1, A549, and A498 bind mannose.[71] The sugar-free nanoprobe NP **1** did not bind to any cells in our study, evidence to the importance of intrinsic carbohydrate−protein interactions involved and the exclusion of nonspecific interactions as the cause of binding. The wealth of new information generated on the sugar-binding preferences of these cell lines can be very useful for cancer research. Although some of the receptors responsible for binding are not determined yet, the magnetic nature of MGNPs can help facilitate the enrichment and identification of carbohydrate receptors on these cells in the future through magnet-mediated separation.

Establishment of MR Responses as Molecular Signatures for Full Differentiation of All 10 Cell Lines via LDA Analysis. With the diverse MR signature in hand, we examined whether it was possible to differentiate all 10 cell lines. This was a particularly stringent test due to the large number of cell lines being analyzed using only five types of MGNPs. In order to accomplish this, linear discriminant analysis (LDA), a statistical method for classification of groups of objects, was employed.[35] LDA converts the Δ*T*2 values of each cell line to canonical linear discriminants (LDs), which are linear combinations of the original data weighted by coefficients producing the greatest analyte discrimination. LDA is a powerful technique, which has been successfully applied to the detection of a variety of targets including carbohydrates, proteins, and cells.[2,35,36,72−74] All *T*2 changes (6 types of NPs, 10 cell types, 8 repetitions) at each cell concentration were submitted to LDA, and LDs were generated. On the basis of the LDA patterns, the 10 cell lines were easily clustered into 10 respective groups (Figure 5). At the 10^5 cells/mL concentration, the first three LDs contain 49.5, 25.3 and 17.5% of the variations respectively, which account for 92.3% of the total variations. Validation of the LDA was carried out using a jackknife matrix method,[75] where all but one measurement out of each group was treated as a new training set. The group memberships of the omitted observations

(70) Satelli, A.; Rao, P. S.; Gupta, P. K.; Lockman, P. R.; Srivenugopal, K. S.; Rao, U. S. *Oncol. Rep.* **2008**, *19*, 587–594.
(71) Chandrasekaran, S.; Tanzer, M. L.; Giniger, M. S. *J. Biol. Chem.* **1994**, *269*, 3367–73.
(72) Zhang, T.; Edwards, N. Y.; Bonizzoni, M.; Anslyn, E. V. *J. Am. Chem. Soc.* **2009**, *131*, 11976–11984.
(73) Jagt, R. B. C.; Gomez-Biagi, R. F.; Nitz, M. *Angew. Chem., Int. Ed.* **2009**, *48*, 1995–1997.
(74) Miranda, O. R.; You, C.-C.; Phillips, R.; Kim, I.-B.; Ghosh, P. S.; Bunz, U. H. F.; Rotello, V. M. *J. Am. Chem. Soc.* **2007**, *129*, 9856–9857.
(75) Yang, M. C. K.; Robinson, D. H. *Understanding and Learning Statistics by Computer*; World Scientific Publishing Company: Hackensack, NJ , 1986.

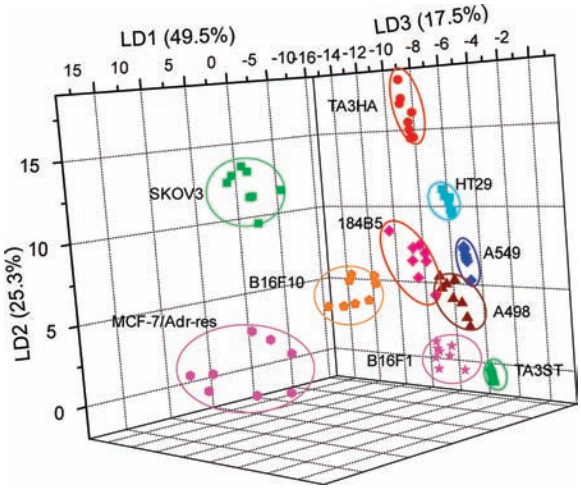

Figure 5. LDA plots for the first three LDs of $\Delta T2$ patterns obtained with the MGNP array upon binding with the 10 cell lines (10^5 cells/mL). Full differentiation of the 10 cell lines was achieved.

were then predicted on the basis of the new training set, which were accurately classified in all the cases tested. This highlights that, despite the simple structures of the monosaccharides utilized, the $T2$ changes of the MGNP array can be employed as characteristic molecular signatures for each cell line.

Next, the possibility of identifying cell lines with unknown identity was explored. Two cell lines out of the 10 were randomly selected as unknowns and submitted to binding with the six NPs. On the basis of the resulting $T2$ changes, the unknowns (unknown 1, MCF-7/Adr-res, and unknown 2, A549) were classified to the groups previously generated. Both unknowns were correctly identified, attesting to the reliability of the analysis (Figure S8, Supporting Information).

Detection of Cancer Cells vs Normal Cells Based on the MR Signature. A major hurdle for cancer treatment and early cancer detection is the identification of pertinent cellular signatures to allow the differentiation of normal cells from their cancerous counterparts. We envision that this can be achieved by analysis of the respective cellular characteristics toward carbohydrate binding. As a proof-of-principle, the $T2$ changes of the breast cancer MCF-7/Adr-res cells vs those of the normal breast endothelial cells 184B5 upon MGNP binding were examined in detail. As the trend of binding is the same qualitatively at both cell concentrations, we focused mainly on $T2$ changes at 10^5 cells/mL. The interactions with Man-MGNP **2**, Fuc-MGNP **4**, and GlcNAc-MGNP **6** were found to be very similar between the two cell lines (Figure 6a). However, the MCF-7/Adr-res cells caused a significantly larger $\Delta T2$ upon binding with Gal-MGNP **3** as compared with that of the normal breast cells 184B5, which enabled easy detection of breast cancer cells. This was corroborated by evidence from the literature that MCF-7/Adr-res cells contain the cancer-specific galactoside binding galectins-4, -7, and -8, which are absent in noncancer cell lines.[70] Modification of the galactoside ligand structures[76] as well as optimization of ligand density and nanoparticle surface chemistry can further improve the selectivity in binding for future *in vivo* applications.

Differentiation of Closely Related Isogenic Cancer Cells Including Metastatic Cancer Cells. Besides the differentiation of cancer vs normal cells, the MR data also enabled the distinction between closely related isogenic sublines of cancer cells. Isogenic cancer cells are derived from the same parent cell line, presenting significant challenges for identification. One example is the mouse mammary carcinoma cell-lines TA3HA and TA3ST. These two types of cells originated from the same parent cell line with TA3HA expressing the mucin-like cell surface glycoprotein epiglycanin absent in TA3ST.[77] Despite this subtle difference, TA3HA showed significantly stronger interactions with the Fuc-MGNP **4** and Sia-MGNP **5** (Figure 6b).

Other examples of closely related cells are the widely used B16F10 and B16F1 mouse melanoma cells, where no qualitative differences in protein composition, galactose or sialic acid content on the cell surface, or the membrane fluidity were observed before.[78] The quantitative nature of the MGNP approach uncovered the subtle difference between these two cell lines with B16F10 showing larger $T2$ change ($P < 0.00001$) upon binding with Gal-MGNP **3** as compared to B16F1 (Figure 6c), which is likely due to the higher level of galectins expressed on B16F10 cells.[24] This is consistent with the observation that galactoside mimetics were more potent in preventing the adhesion of B16F10 to extracellular matrix component than that of B16F1.[24] B16F10 also caused larger $\Delta T2$ with Man-MGNP **2** and Fuc-MGNP **4** at 10^5 cells/mL. These results indicate that, despite the overall similarity, there are quantitative changes in carbohydrate binding between the B16F1 cells and its metastatic variant B16F10.

Cellular Uptake and Biocompatibility of MGNPs. In order to gain insights into how MGNPs interact with cells, cellular staining experiments were performed. Besides their properties as MRI contrast agents, MGNPs can be visualized by Prussian blue staining, which yields an intense blue color upon reaction with the magnetite core of MGNPs, allowing easy tracking of the particles. As an example, B16F10 cells were incubated with MGNPs (20 μg/mL), washed extensively with buffer to remove all unbound nanoparticles, and stained with Prussian blue. As Man-MGNP **2**, Gal-MGNP **3**, and Fuc-MGNP **4** caused the biggest $T2$ changes when incubated with B16F10, strong blue stains were observed both on cell surfaces and inside the cells, suggesting a significant cellular surface binding and cellular uptake (Figure 7a−c). In contrast, the nonbinding GlcNAc-MGNP **6** and control particle NP **1** without any carbohydrates did not show much staining (Figure 7d,e). The same phenomena were observed with other cell lines as well (Figure S9, Supporting Information). The correlations between Prussian blue staining and $T2$ changes proved that the MR changes were indeed due to NP binding with the cells. The selective uptake and intracellular accumulation of specific MGNPs in cancer cells and the ability of MGNPs to differentiate normal cells from tumor cells bode well for further development of MGNPs as vehicles for targeted drug delivery[79,80] and magnetic-induced hyperthermia therapy of cancer.[81]

(76) Delaine, T.; Cumpstey, T.; Ingrassia, L.; Le Mercier, M.; Okechukwu, P.; Leffler, H.; Kiss, R.; Nilsson, U. J. *J. Med. Chem.* **2008**, *51*, 8109–8114.
(77) Miller, D. K.; Cooper, A. G. *J. Biol. Chem.* **1978**, *253*, 8798–8803.
(78) Raz, A.; McLellan, W. L.; Hart, I. R.; Bucana, C. D.; Hoyer, L. C.; Sela, B. A.; Dragsten, P.; Fidler, I. J. *Cancer Res.* **1980**, *40*, 1645–1651.
(79) Davis, B. G.; Robinson, M. A. *Curr. Opin. Drug Disc. Dev.* **2002**, *5*, 279–288.
(80) Yamazaki, N.; Kojima, S.; Bovin, N. V.; André, S.; Gabius, S.; Gabius, H.-J. *Adv. Drug Delivery Rev.* **2000**, *43*, 225–244.
(81) Thiesen, B.; Jordan, A. *Int. J. Hypertherm.* **2008**, *24*, 467–474.

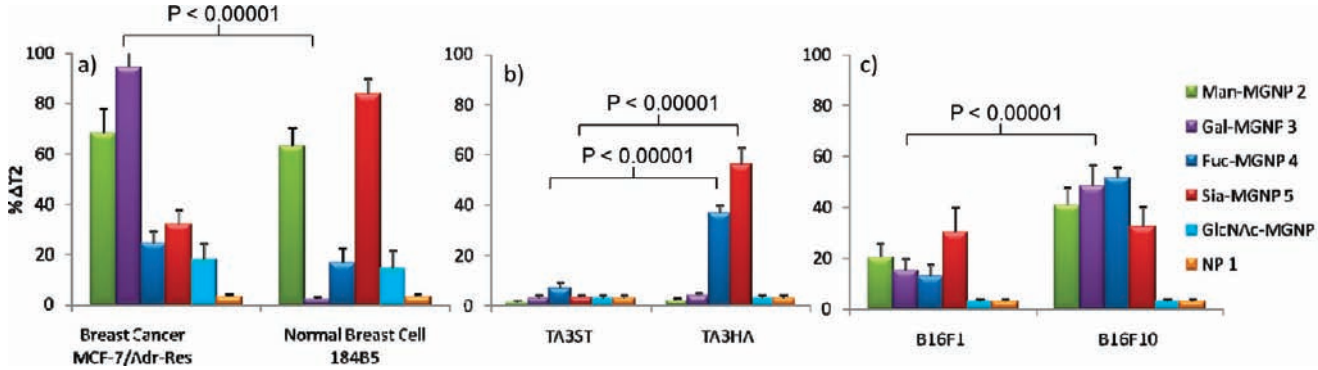

Figure 6. Percentage changes of *T*2 relaxation time (% Δ*T*2) obtained upon incubating MGNPs **2**−**6** or the control NP **1** (20 μg/mL) with (a) breast cancer MCF-7/Adr-res vs normal breast cell 184B5; (b) TA3ST vs TA3HA cell lines; and (c) B16F1 vs B16F10 (10^5 cells/mL). Significant differences in binding with MGNPs were observed, thus differentiating these cell lines.

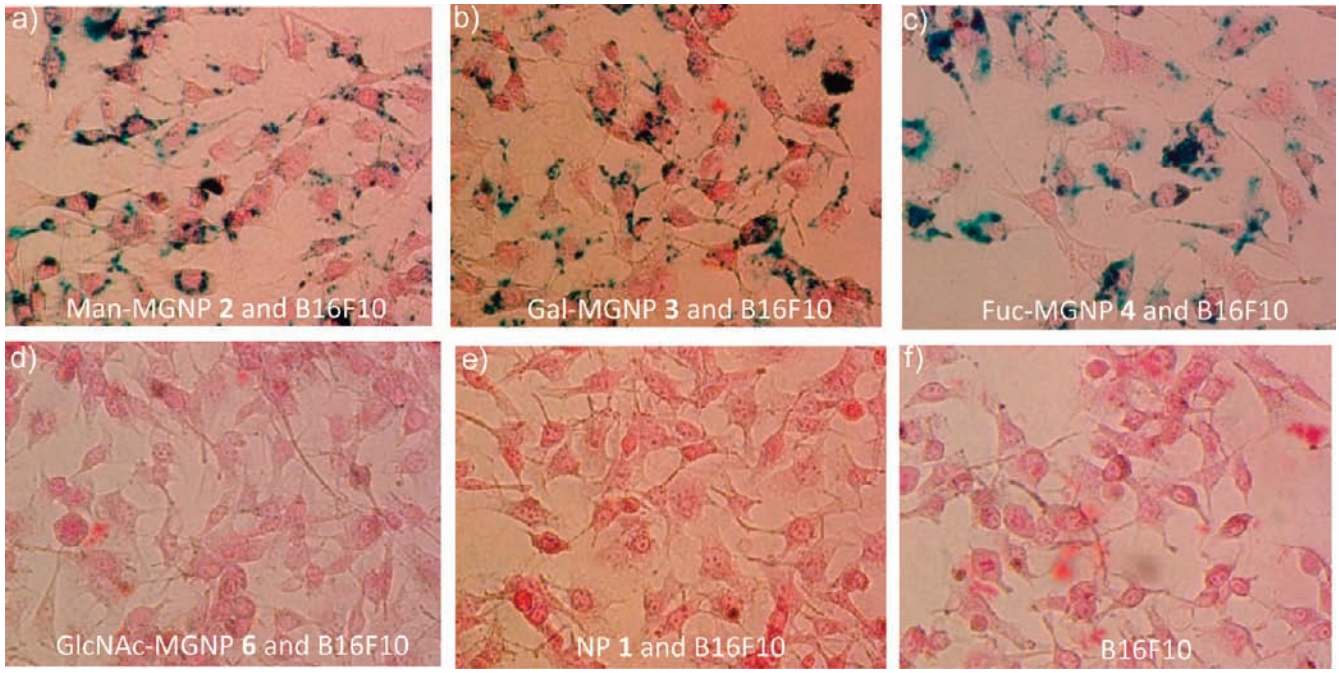

Figure 7. Prussian blue staining images of 20 μg/mL of (a) Man-MGNP **2**; (b) Gal-MGNP **3**; (c) Fuc-MGNP **4**; (d) GlcNAc-MGNP **6**; and (e) control NP **1** incubated with B16F10 cancer cells after unbound particles were removed by washing; and (f) B16F10 cells. The images clearly indicate the high intracellular uptake of Man-MGNP **2**, Gal-MGNP **3**, and Fuc-MGNP **4**. No Prussian blue stains were visible with the nonbinding GlcNAc-MGNP **6** and the control NP **1**, proving the selectivity in binding.

Next, we examined the toxicity of the MGNPs toward the cells by 3-(4,5-dimethylthiazol-2-yl)-2,5-diphenyltetrazolium bromide (MTT) cell viability assays. Incubation of cells with different MGNPs for one week did not show any negative effects on cell viability as compared with untreated cells (Figure S10, Supporting Information). This demonstrates that the MGNPs are biocompatible and can be used as safe MRI contrast agents.

Antiadhesive Properties of MGNPs. Tumor metastasis is associated with poor prognosis of cancers.[82] One of the critical steps in metastasis is the adhesion of circulating tumor cells to endothelium at the target location. It has been demonstrated that cell adhesion inhibitors can be a potential treatment for metastatic diseases.[83−85]

The MRI signature from MGNPs provides detailed information on how tumor cells interact with each carbohydrate, which is valuable for guiding the development of antiadhesive agents, as the strongly binding MGNPs can reduce the adhesion of cancer cells to the matrix by blocking the cell surface receptors. According to the MRI signature, Gal-MGNP **3** interacted strongly with B16F10 cells, which led us to measure its antiadhesive properties as a proof-of-principle study. Upon incubation of B16F10 cells with Gal-MGNP **3**, the number of cells adhering to the surface was reduced by more than 50% (Figure 8). In contrast, the nonbinding NP **1** showed little effect on cell adhesion. Modification of the monosaccharide ligands immobilized on

(82) Kawaguchi, T. *Current Drug Targets: Cardiovasc. Haematol. Disorders* **2005**, *5*, 39–64.
(83) Rojo, J.; Diaz, V.; de la Fuente, J. M.; Segura, I.; Barrientos, A. G.; Riese, H. H.; Bernad, A.; Penadés, S. *ChemBioChem* **2004**, *5*, 291–297.
(84) Zhu, D.; Cheng, C.-F.; Pauli, B. U. *J. Clin. Invest.* **1992**, *89*, 1718–1724.
(85) Meromsky, L.; Lotan, R.; Raz, A. *Cancer Res.* **1986**, *46*, 5270–5275.

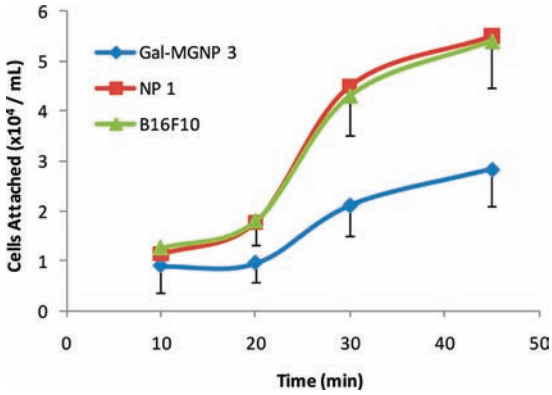

Figure 8. Adhesion of mouse melanoma B16F10 cells (~5 × 10^4 cells/mL) to the surface was significantly reduced by incubation with Gal-MGNP **3** (blue line), while the control NP **1** (green line) had no effect on cell adhesion as compared to cells without treatment with any NPs (red line). Error bars indicate standard deviations (triplicate readings).

MGNPs may strengthen the binding with the cells, further enhancing the antiadhesive effects.

Conclusion

A new approach based on the multichannel MR responses of MGNPs to qualitatively and quantitatively map the carbohydrate-binding characteristics of a variety of cancer cells was developed. Validated through binding with a series of lectins and a well-characterized *E. coli* system, the carbohydrates immobilized on MGNPs were found to retain their biological recognition and binding specificities. Although the monosaccharides utilized in this study are fairly simple in structures and multiple cells may bind with the same carbohydrate, the selective carbohydrate−receptor binding with the MGNP array amplified the small structural differentials. The resulting combined array responses allowed the detection of cancer cells as well as the differentiation of closely related isogenic cancer cell subtypes without detailed prior knowledge on endogenous carbohydrate receptors, while the wealth of information generated and magnetic nature of the MGNPs can facilitate future identification of the receptors. The LDA pattern recognition method was applied to decipher the glyco-codes of tumor cell binding, which may be a useful and general protocol to analyze carbohydrate−receptor interactions.

The strongly binding MGNPs were found to be internalized by tumor cells, and they significantly reduced the cancer cell adhesion. As the MGNP array measures the physiologically related carbohydrate−receptor interactions, which are involved in a variety of cellular functions including endocytosis, cell-matrix and cell−cell communications, the knowledge gained from this new addition to the glyco-nanotechnology toolbox can enhance our understanding of cancer cell functions. This can provide leads for further ligand optimization to improve the specificity in carbohydrate-receptor recognition, which in turn can enable the application of MGNPs for *in vivo* cancer detection through MRI in the future.

Acknowledgment. We thank E. Caneva from Centro Interdipartimentale Grandi Apparecchiature (C.IGA University of Milan), L. Polito and S. Ronchi from ISTM-CNR (Milan) for technical help with HRMAS experiments, and Dr. John Hilkens (Netherlands Cancer Institute) for kindly providing the two murine mammary carcinoma cell lines (TA3-HA, TA3-ST). This work was partly supported by a CAREER award from NSF (X.H.), a predoctoral fellowship from the American Heart Association (K.B.), and the Departments of Chemistry and Radiology, Michigan State University.

Supporting Information Available: (1) Experimental procedures for synthesis of the MGNPs; (2) characterization of the MGNPs; (3) MGNP-lectin binding assays; (4) MGNP−*E. coli* binding studies; (5) LDA plots at 10^6 cells/mL; (6) Prussian blue staining images, and (7) NMR spectra for all new compounds. This material is available free of charge via the Internet at http://pubs.acs.org.

JA100455C